THE UNIVERSITY OF
MELBOURNE

Towards a Higher Resolution Gamma Camera

Christopher James Wong

Honours Report
November 10, 2003

Supervisors:Dr. Roger Rassool
Dr. Max Thompson

School of Physics

The University of Melbourne

Submitted as partial fulfilment of the requirements for a Bachelor of Science (Honours)

I authorise the Chairman of the School of Physics to make copies of this report for research, study or instruction.

signature.....

Abstract for the Report

Applications for the gamma camera include a modality for non-invasive medical imaging, a useful technique allowing non-invasive medical examination. This is done by the camera detecting radioactive isotopes (typically ^{99m}Tc) placed into the body.

Another, exciting application is the ability to use as the large area detectors in a proposed mobile land-mine detection system by detecting the resultant γ-radiation given off when the nitrogen in the explosives is exposed to neutrons. By mapping the nitrogen location under ground with a large γ-ray detector, land-mine removal can be made safer and faster.

A gamma camera is comprised of a large-area scintillator crystal, coupled to an array of photomultiplier tubes (PMTs) which detect the reactions that occur when radiation hits the crystal. Using Anger logic the location of interaction of a γ-ray from a sample can be found with an accuracy of a few mm.

The location of an event can be found to a good degree of accuracy by use of 'Anger Logic'. This allows resolution better than what can be achieved by the physical size of the PMTs.

This project examines the resolution of the camera by use of Anger logic and the feasibility of it's improvement by increasing in the number of tubes analysed. This will be done by first analysing the properties of a gamma camera, and then modelling to examine this feasibility.

A point to consider is that at high count rates, there will be pile-up in signals received, which can distort the imaging produced. How this can affect results will also be simulated.

Acknowledgements

I would like to thank the following people:
Dr. Roger Rassool
Dr. Max Thompson
Tim Dyce
Leighton Smith
Viliami Takau
Rebecca Scott
Gareth Jones

for helping me as I worked on this project
Also everyone for being there.

Contents

List of Figures

List of Tables

1 Introduction

Gamma cameras are used as a method of non-invasive medical imaging. With such a tool, significant information on internal bodily structures can be obtained, allowing accurate diagnosis and treatment.

Since this technique has been in use for considerable time, there are a number of obsolete units available at minimal cost. This raises the possibility of using one as the γ-ray detector for a mounted mobile land-mine detection system. This would be achieved by the mapping of sub-terrainian explosive location by detection of γ-rays following thermal-neutron capture of the associated nitrogen.

A Gamma camera is a device comprised of an array of PMTs, which view a continuous, thin layer of scintillation material (such as NaI) in which the γ-rays interact from which the PMTs detect emitted visible photons. This light is emitted when γ-rays interact with the scintillator. When used, the scintillator is shielded by a lead collimator, so that only beams of γ-rays that are normal to the surface are received and detected. Figure 1 shows this. The size of the matrix of holes in the collimator are typically 1 mm in diameter and the PMTs are hexagons with a radius of $\approx$ 30–35 mm.

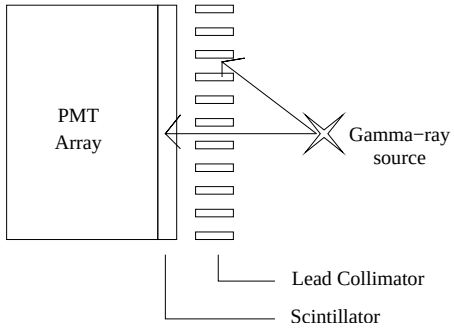

Figure 1: Lead collimator only allows parallel rays into the scintillator.

One can determine the approximate location where an incident γ-ray interacted with the scintillator took place by observing which PMT receives the most light. From this, we can determine the nearest PMT as an estimate of the region of the interaction. This gives a resolution of the size of the PMT. However, one might suggest that the PMTs are fairly large, and the using many small PMTs is prohibitively expensive.

By use of a technique known as Anger logic, it is possible to calculate from the data collected from the PMTs the location of the region where the photon producing interaction took place. This allows significantly better resolution that is obtained by simply locating the nearest PMT.

As a result of the design, every PMT in an array will observe light from the interaction of the γ-ray in the crystal. The amount of light from any detected γ-ray interaction in a given PMT will depend on the distance of the PMT from the location where the interaction took place. For example, in figure 2 we see that an interaction has taken place near the PMT #2, so it will receive the greatest amount of light. Since the event takes place slightly

to the left of PMT #2, PMT #1 also receives some of the light, but less than PMT #2. PMT #3 on the right is further away and receives even less light from this interaction than PMT #1.

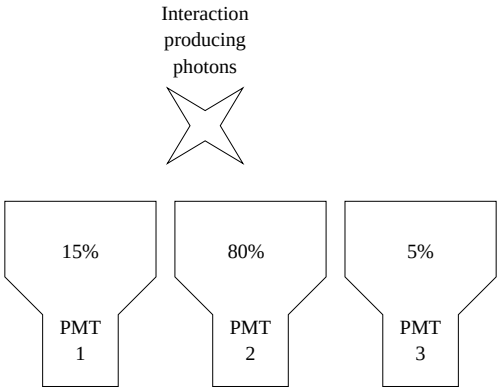

Figure 2: PMTs receive a number of photons based on how far away they are from an interaction.

An important factor in these measurements is the resolution obtained. With better resolution, one can make better judgement on the actions to be taken during surgery, or when locating mines. For medical purposes, one would need a high level of resolution, in order of millimetres. For clearing land-mines (typically 5 cm in diameter), a resolution of order in centimetres would be sufficient.

Typically, the PMTs used to detected the interaction location are that one with the greatest amount of light received and the six PMTs which immediately surround it (these six are known as the first ring of PMTs). The purpose of this project was to investigate the possibility of improving the resolution of a pencil beam onto the gamma camera by increasing number of PMTs over which Anger logic was applied.

To do this, I planned to experimentally verify the Anger logic using a gamma camera with a known radiation source, and then use this as a model for a computer simulation to investigate methods that may improve the resolution. In addition, I planned to examine the potential problems to Anger logic that could arise when multiple signals are detected simultaneously.

2 Theory

2.1 γ-Ray Interaction

γ-rays interact with material in 3 ways: Compton Scattering, Photo-electric Effect and Pair Production. We are concerned mainly with the Photo-electric effect for gamma cameras, although the effects of Compton Scattering can be seen in some cases. Pair production is not considered in this report, as the energies required for it to occur are rare. However, with other sources of radiation (eg. γ-rays that result from nitrogen after interactions with neutrons), the process will become important.

All three interactions give rise to electrons that move though the NaI crystal lattice. NaI has a high Z, making it effective at detecting γ-rays. For medical applications, ^{99m}Tc is used, and the electrons have a path length of $\approx$ 0.1 mm in NaI. For neutron-capture γ-rays (8–10 MeV) from nitrogen, the photoelectrons have an estimated range of $\approx$15 mm. In NaI, the range of an 662 keV photoelectric electron such as from ^{137}Cs used in this experiment is $\approx$1 mm [NIS].

This path length of the electrons will act as a limit to the resolution. Light due to the interaction will be emitted from a region of this length that the electrons can reach, so it is impossible to locate the site of the interaction to a degree of accuracy greater than this. The practical limit to measurements made will therefore depend on the source of γ-rays that are used.

As the electron travels though the lattice, it will excite near-by atoms into higher energy states, and lose energy in the process. A 1-MeV electron can excite in order of 10,000 atoms in this process. The excited atoms will quickly de-excite back to their ground states, emitting photons in the visible and UV spectra. Figure 3 shows an example of this.

The light from the de-excitations can be detected by a PMT, resulting in a pulse of a certain size, proportional to the energy that the initial γ-ray gave to the electron and the distance of the PMT from the interaction. Those pulses are then recorded by the MCA as a spectrum. After many events, the spectrum will have a particular shape according to the amount of light received by the PMT for each event. A spectrum for ^{137}Cs in NaI from the camera for example, looks like figure 4.

In figure 4 the peaks from right to left are the photoelectric peak, the compton edge, the backscatter peak and the X-ray peak due to the 32 keV X-rays that are also emitted for the source.

By using an array of PMTs, we can estimate the approximate location of a γ-ray event. The simplest way is to see in which PMT the largest signal is recorded. Thus, the location of the source in the X and Y dimensions can be determined to within the size of the PMT. As mentioned earlier, one way of increasing the resolution would be to make the PMTs smaller. However, this is difficult and not very practical. Fortunately, there is another solution, achieved by placing all the PMTs behind one large block of scintillation material and using Anger logic.

Not all PMTs will record the same amount of light. Some PMTs will receive a greater amount of light because they lie closer to the initial reaction than others. As a result the

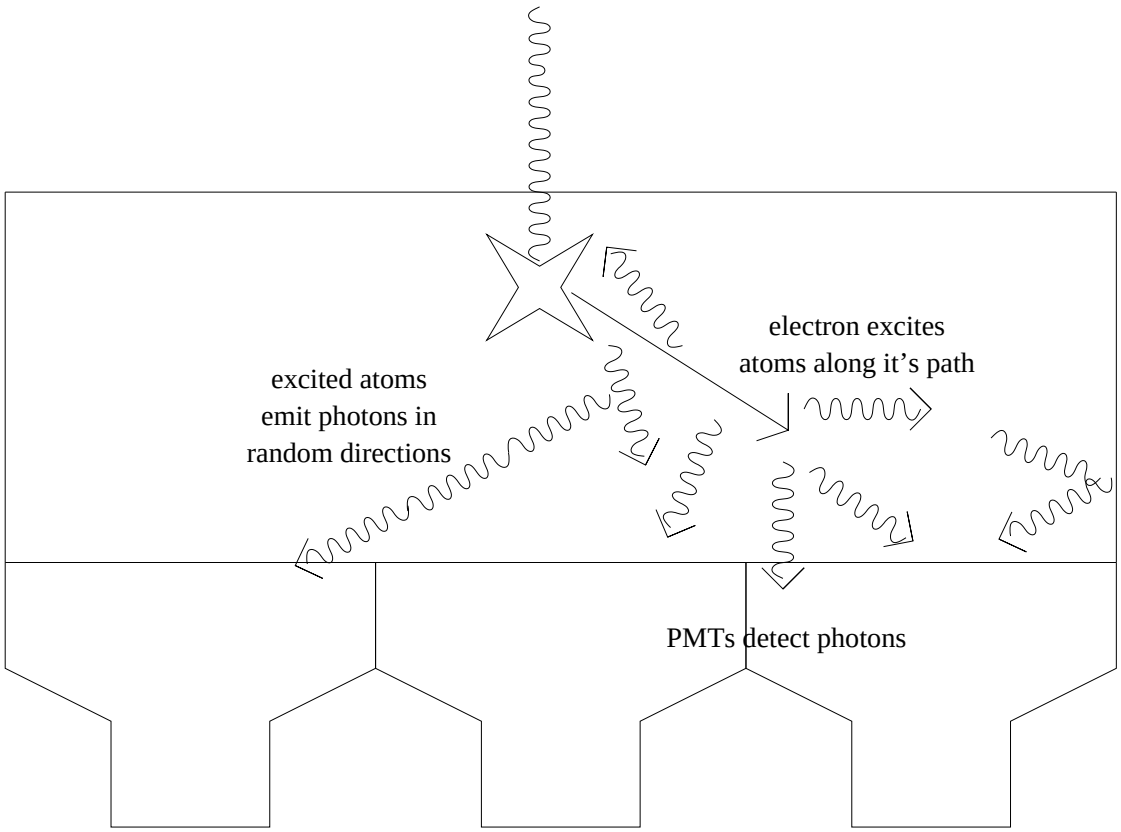

Figure 3: Photons are emitted from atoms excited due to passing electron.

spectrum will be contracted to lower channels as the amount of light decreases compared to other PMT's in the array. As a result, we will see the peaks attributed to photo-electric effects, etc. at apparently higher energies in PMTs close to the source relative to those further. Figure 3 shows how this is possible.

The MCA records a spectrum based on the amount of light it receives from each event. Figure 5 shows what the spectrum typically looks like (the spectra have had the background counts subtracted). Peaks in these figures represent the the different interactions, and last peak (one furthest to the right) is the peak due to photoelectric events. For the case where the PMT is placed directly in front of the beam (Figure 5, bottom), the photoelectric peak appears in a channel representing a high energy, meaning a high intensity of light. When the PMT is some distance from the beam (Figure 5, top), the spectrum has the same shape, but all the counts are recorded at lower channels. This indicates that there is less light observed by the PMT for these events. From this, we can conclude that a PMT further from the beam will receive less light compared to a PMT near the beam.

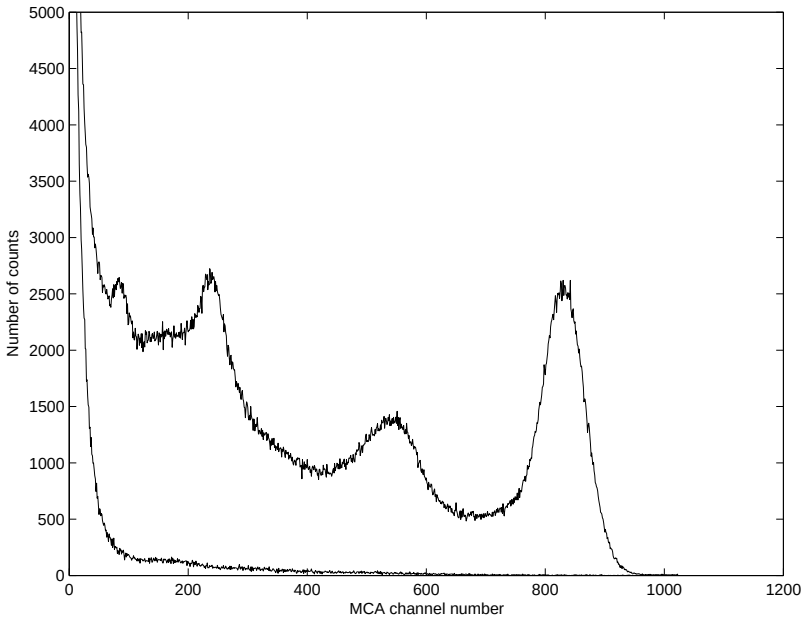

Figure 4: Typical spectra from a ^{137}Cs source onto a NaI scintillator. The top curve is the spectrum from the source, the bottom curve is the counts due to the background.

2.2 Anger Logic

Anger logic was developed by Hal Anger in late 1950's [Ang66]. The technique is applied to many different applications, but here we are concerned with it's use with an array of PMTs: something Anger worked on in relation to medical imaging.

The premise of Anger logic is to use the signals simultaneously detected from many PMT's arranged in a known formation to determine the location of events within the scintillator. By comparing the amount of light received at each PMT, it is possible to achieve an accuracy in location determination better than the physical size of the individual PMT.

The formula for Anger logic is shown below. Separating the PMT array into X and Y dimensions, the light from each PMT is weighted linearly according to it's distance from a chosen origin.

The anger logic used here can be described as:

$$\frac{\sum X_{PMT} \times E_{PMT}}{\sum E_{PMT}} = X_{source}$$

X_{PMT} is the location of the PMT in the X direction,
E_{PMT} the energy that the PMT received.
X_{source} is the estimated location of the beam in the X direction.

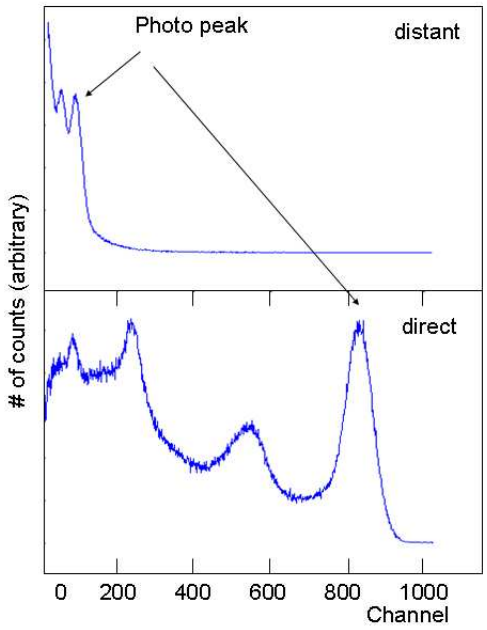

Figure 5: MCA spectra for ^{137}Cs recorded from a PMT in the first ring of PMT's from the source (top) and for a source centred over the radiation source (bottom).

Similarly for the Y location. This is very simple in principal, but provides a very useful technique. Looking at the diagram in figure 6 we see how this works. In this diagram, we have a PMT centred at location X = 5 with the photopeak in channel 700 and the PMT at location X = 10 with the photopeak in channel 250. So therefore we have:

$$\frac{5 \times 700 + 10 \times 250}{950} = 6.32$$

So in this case we would estimate the location of the beam to be at X = 6.32.

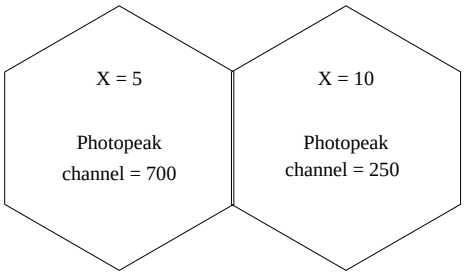

Figure 6: An example of anger logic with 2 PMTs.

3 Experimental Work

3.1 Aim of Data Collection

To determine if it was possible to improve the resolution of the camera, I aimed to observe how quickly the light intensity from a narrow pencil beam of γ-rays at a known location decreased as the distance of a PMT from a source of radiation was increased. All PMTs in the array (with noted exceptions) were measured to determine if they could valuably contribute to the determining the location of the beam.

By applying Anger logic to the data, it should be possible to calculate the location of the incident γ-ray beam, so this will be verified. The rate of light intensity decreasing over distance will later be used to make a computer simulation of the camera.

3.2 Gamma Camera Properties

The gamma camera used in this project was made from an array of regular hexagonal PMTs, each of size $530 \pm 30 mm^2$ (figure 13 is a photo of a PMT used). Forty-nine of these PMT's are arranged and numbered as shown in figure 7. The co-ordinate system used in this report is also shown, and a picture of the camera is in figure 10. Figures 10, 11, 12 and 13 are pictures of the camera and PMTs used in this report.

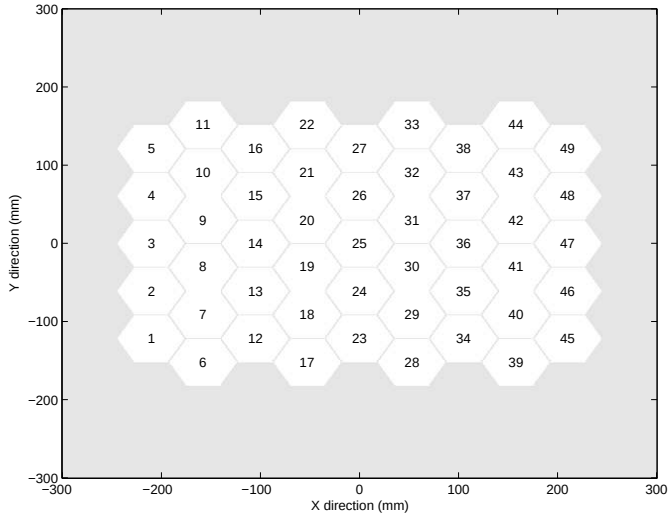

Figure 7: Setup of the PMTs with the co-ordinate system used. γ-rays enter the NaI into the page, and the PMT array faces the NaI crystal from behind.

These PMT's observe a 6-mm thick layer of NaI scintillation material. The technical data of the PMTs used in this project is listed in the appendix.

The source were mounted on a platform that could be moved about to a location of our choice with accuracy of ± 2 mm, which is added to the uncertainty we have in the beam uncertainty already. In figure 8 is a basic diagram of the experimental setup.

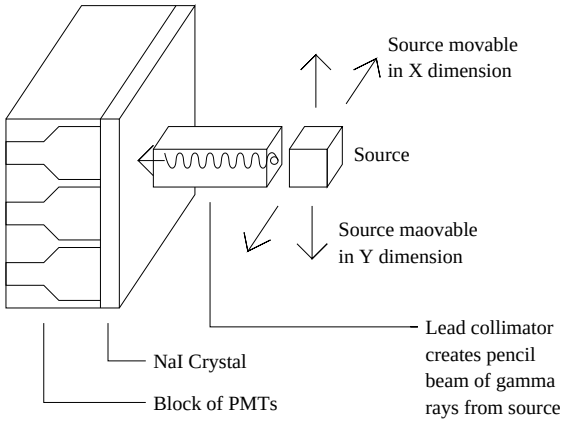

Figure 8: Setup of the camera and the source with collimator.

The source used was ^{137}Cs, collimated to a beam diameter of 4 mm. ^{137}Cs emits 662 keV γ-rays. The source was well shielded by it's own encasing of lead $\approx$4 cm thick, and it was further shielded by lead $\approx$36 cm thick, apart from a small collimated beam to act as a beam source.

All PMT's in the camera were supplied from a single high-voltage power supply, used in the range of 800-1000 V. The output was passed through an amplifier and then to the MCA. The settings on the amplifier and the high voltage varied for each PMT as to normalise the gain. Figure 9 shows the set-up.

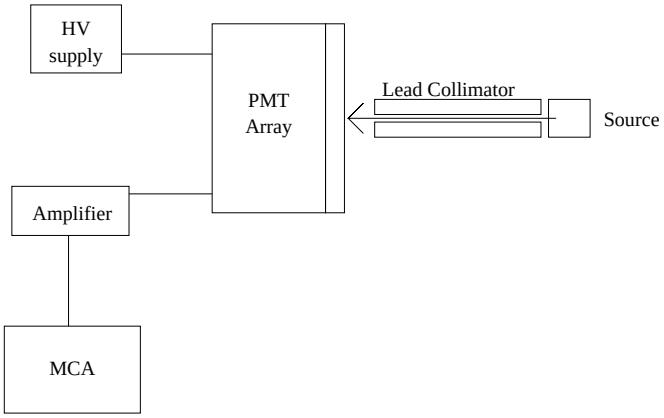

Figure 9: Setup showing electrical components and source configuration.

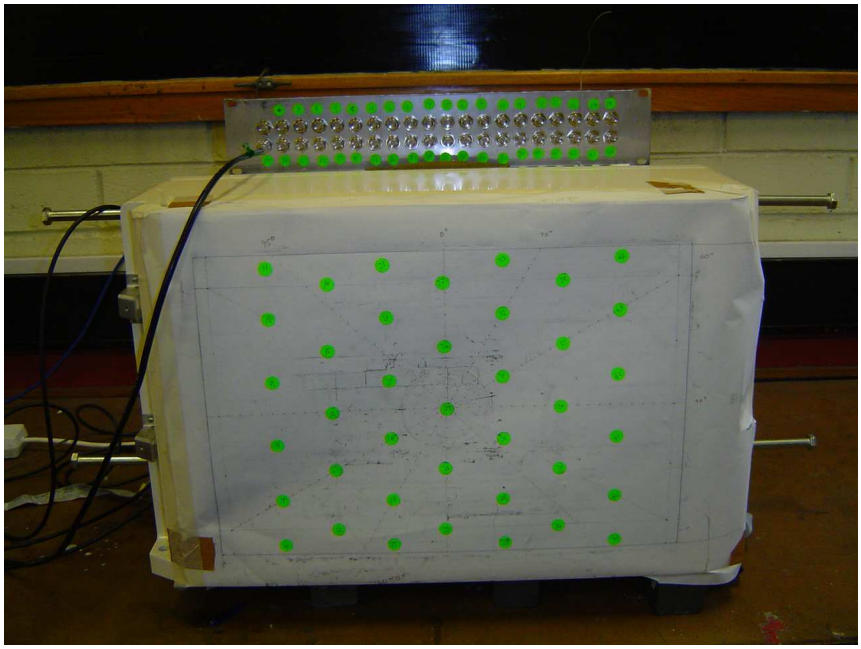

Figure 10: Front of the Gamma camera. The green dots represent the location of the PMTs behind the NaI.

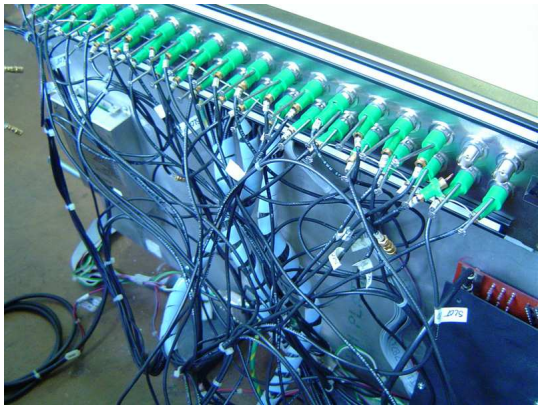

Figure 11: PMT cables attached to a mount.

Figure 12: A picture from behind the array of PMTs.

Figure 13: A close up of a single PMT.

3.3 Method of Data Collection

A pencil beam of 662-keV γ-rays from ^{137}Cs was directed perpendicular to the face of the NaI crystal (figure 9). This beam (4 mm in diameter) was produced using a long Pb collimator.

The procedure was to direct the beam onto a known position of the camera face, and to measure the spectrum from every PMT (except #1–6 and #45–49) in the matrix. In fact this was done for two different locations separated by 30 mm, in an attempt to determine the resolution of the camera.

It was essential that the gain of all PMTs was identical. Thus in a preliminary procedure, using a ^{22}Na source (1.27 MeV and 511 keV γ-rays), the settings of the HV for each tube was recorded in order to normalise the spectra.

3.3.1 The measurement of the performance of each PMT.

The beam of 662-keV γ-ray was directed to the position (-20 ± 2 mm, -7 ± 2 mm) (see figure 7 and the spectrum recorded from each PMT. Each measurement consisted of a spectrum with the source incident and a background obtained by blocking the beam's path to the camera with a 3 cm Pb insert. The background spectrum had no structure and contributed $\approx$8% of the foreground. To determine the response to the defined pencil beam, this background was subtracted form the foreground spectrum. Figure 4 shows a foreground and background spectrum. The beam was moved to a second location (-50 ± 2 mm, -7 ± 2 mm) and the procedure repeated.

In tables 1 and 2 I have listed the location of the photoelectric peak and the % of light that each PMT recived compared to the light it would have received if the source directly over it. The co-ordinate system for the tube locations refers to figure 7. Although I took measurements for all of the PMTs, only those that gave an identifiable photopeak are listed for each location.

PMT no.	X position of PMT (mm)	Y position of PMT (mm)	Peak Location (MCA channel no.)	% of Light
18	-52.5	-90.92	25 ± 2	3.0 ± 0.3
19	-52.5	-30.31	289 ± 2	37.4 ± 0.4
20	-52.5	30.31	169 ± 2	19.7 ± 0.5
24	0	-60.62	116 ± 2	14.0 ± 0.3
25	0	0	608 ± 2	72.5 ± 0.5
26	0	60.62	48 ± 2	5.6 ± 0.3
30	52.5	-30.31	36 ± 2	4.4 ± 0.3
31	52.5	30.31	27 ± 2	3.2 ± 0.3

Table 1: Photo-peak channel and energy for a Cs-137 source at Position 1 (-20 mm, -7 mm), taken 29/9/2003

PMT no.	X position of PMT (mm)	Y position of PMT (mm)	Peak Location (MCA channel no.)	% of Light
13	-105	-60.62	43 ± 2	4.6 ± 0.3
14	-105	0	96 ± 2	11.4 ± 0.3
15	-105	60.62	23 ± 2	2.9 ± 0.3
18	-52.5	-90.92	33 ± 2	4.0 ± 0.3
19	-52.5	-30.31	585 ± 2	75.6 ± 0.6
20	-52.5	30.31	299 ± 2	34.8 ± 0.4
21	-52.5	90.92	33 ± 2	4.5 ± 0.3
24	0	-60.62	57 ± 2	6.9 ± 0.3
25	0	0	174 ± 2	20.8 ± 0.4
26	0	60.62	29 ± 2	3.4 ± 0.4

Table 2: Photo-peak channel and energy for a Cs-137 source at Position 2 (-50 mm, -7 mm), taken 30/9/2003

The data in the tables is plotted as a function of distance of PMT from the source. The results give an indication of the light cone shape that we obtain. Figure 14 (for table 1) and figure 15 (for table 2).

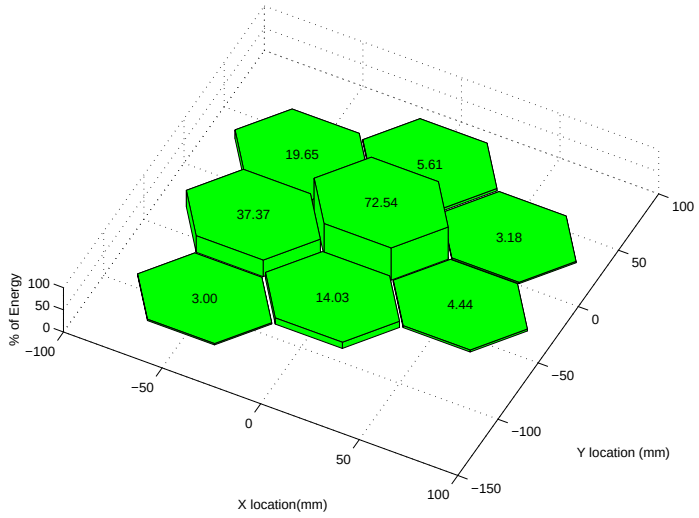

Figure 14: Energy ratios of measurement at position 1 (-20 mm, -7 mm)

3.4 Data Analysis

From this data, we can see that we get very little information from tubes beyond the first ring surrounding the PMT with the highest count rate. Using the data from tables 1 and 2, it is possible to plot a decay curve of source distance against light ratio, as shown on the RHS of figure 16.

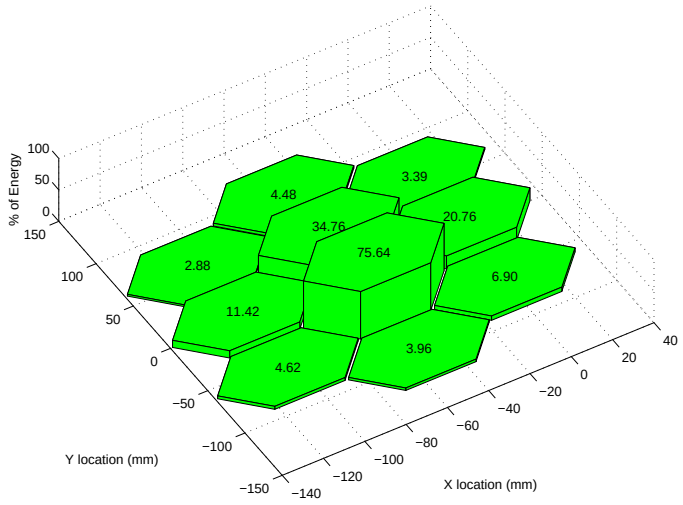

Figure 15: Energy ratios of measurement at position 2 (−50 mm, −7 mm)

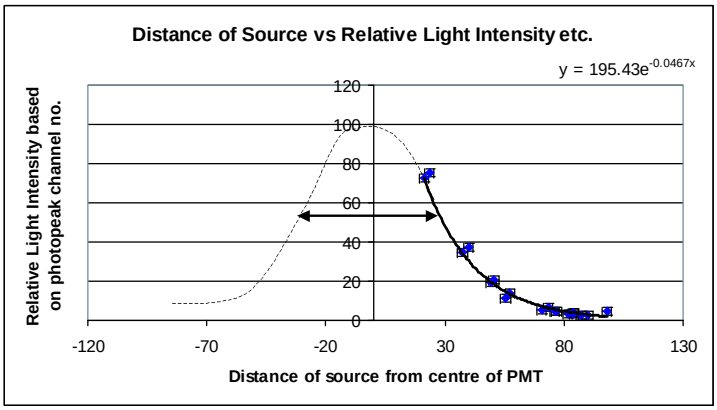

Figure 16: Rate of light intensity decay against distance on the RHS, and a extraperlation to 0 and reflection on the LHS.

If we extrapolate the graph to a distance = 0 mm, we see it crosses at 195.43 rather than 100 as it must, since the light is normalised to the light output at the central point. Consequently, the shape of the curve must be similar to the dashed line.

Reflecting the curve derived from the data on the RHS of the figure, gives the plot shown in figure 16. The shape of this is similar to a normal distribution, and if we take the FWHM of this distribution, it is approximately equal to the diameter of a PMT (≈60 mm). With this in mind, it would appear that the size of the PMTs seems to have been chosen with this point in mind. At such a size, we would have it so that the system was designed to obtain ≈50% of the the centre PMT's light spread out into the next ring.

The channel number of the photoelectric peak is the indication of the light intensity reaching a particular PMT. The dependence of this as a function of distance of the PMT (centre) from the source position (figure 16 showed two important facts.

1. The dependence of the observed light intensity varied as:

$$LightIntensity = 195.43e^{-0.0467 \times distance}$$

where distance is in units of mm and Light Amplitude is a ratio compared to that when distance = 0.

2. As a consequence, and consistent with the spectra obtained, only tubes within 8-10 cm of the source gave a discernible photoelectric peak

In practice this means that the number of tubes that can be used in the Anger logic calculation is limited. In practice, if the event occurs directly in front of one tube, only the inner ring of 6 tubes can be used in determining the event location.

In quantifying this I conclude that each tube in this ring receives $(6.0 \pm 0.2\%)$ of the total light.

If we apply Anger logic to the data above, we get the following table 3.

Source position (mm)	Calculated X position (mm)	Actual X position (mm)	Calculated Y position (mm)	Actual Y position (mm)
Measurement 1 $(-20, -7)$	-16.5 ± 4.8	-20 ± 2	-6.9 ± 3.4	-7 ± 2
Measurement 2 $(-50, -7)$	-48.7 ± 7.0	-50 ± 2	-1.4 ± 3.0	-7 ± 2

Table 3: Calculated source location using anger logic on measurement data.

Taking the uncertainty in initial position to be ± 2 mm and an uncertainty in calculated position to be the same, the results above are reasonably satafactory. The only one that is strange is the Y location for the second measurement. It is odd that this one is off by so much when the Y location for the first measurement works so well. The X positional data for the second measurement also looks good, making it less likely (but not impossible) that the data recorded and used was incorrect.

The actual X, Y position maybe in error by ± 2, so that the calculated values of both measurements are satisfactory. The X co-ordinate as calculated agree within the errors. The Y co-ordinate from measurement 2 is right at the limit of the errors. It seems possible that the difference may be actually result from the inability to incorporate data from tubes in the next adjacent ring.

3.5 Conclusions from the Experimental Work

The ability to observe the photopeak limits the range of included PMTs. However, it should be noted that the ability to resolve the photopeak is not the ultimate limitation. It is the integrated spectrum (after background removal) that indicated the light intensity at the PMT, and in a well set up system this would be used in the Anger calculation, leading to a better resolution. This improvement will be considered in the simulation section.

4 Computer Simulation

4.1 Aims of the Simulation

A major part of this project required significant computer modelling of the detector so as to simulate as closely as possible the situation measured before in the experimental work. This would then be used as a basis to make further predictions.

The first requirement of the model was to accurately predict the light distribution in the scintillator for subsequent comparison with the experimental measurements. Shown in figure 17 is the distribution obtained, showing the rate of light decrease for a 7 PMT system. The dimensions of the system were made to match those of the gamma camera used in the experiment. In this false colour image, Red represent regions where the light collected is the brightest and blue the dimmest.

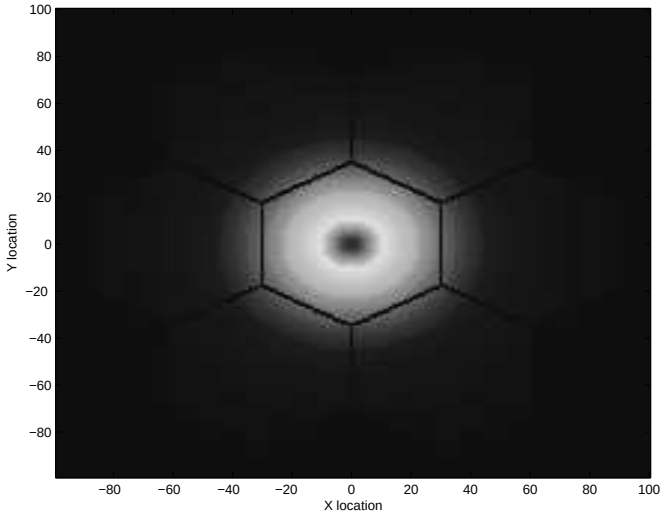

Figure 17: A light cone for a 7 PMT system.

In later revisions of the modelling software, we extended the program to include more than the limited number of 7 phototubes, and this was then used as a basis to test various scenarios. As is explained below, of particular interest was the investigation of whether or not additional accuracy in position reconstruction could be obtained by including weaker signals from distant phototubes.

The decay time in crystal has been a factor ignored until now, it arises because not all of the atoms in the scintillator will de-excite at the same time. As a result, there will be an extended period of time over which the PMTs will be collecting photons. In the experimental measurements, an integration time of 1 μs was applied to each event so as to allow sufficient light collection for the known decay time of NaI (230 ns). Because of the random nature of atomic radiation, it is possible that two or more γ-rays will be incident and interact will the detector at almost the same time. Under these conditions, the array of PMTs will detect photons from both events within the same time-frame. This is known

as pile-up.

The adverse effect of pile-up is that it could possibly give mis-leading positional data. This arise from the fact that each event independently distributes light to a different weighted combination of PMTs. Ignorant of this fact, the crude anger logic will incorrectly decode the position was the weighted sum of the events.

Using the simulations, we aim to look at what kind of effects pile-up can give when simulating anger logic. It is anticipated that in some cases it may be possible to identify that a pile-up event has occurred by examining the time distribution of events and to then deal with the situation accordingly. Furthermore, we intended to simulate how often we can expect pile-up to occur. Details of the computer programs used may be found in the appendix.

4.2 Brief Description of the Program Methods

A series of programs were developed to study the behaviour of the detector. Initially, a simple program was developed to calculate the position of a source given 7 hexagonal PMT with received light based on a simulated light cone (as shown in figure 17). Several potential models for the light distribution were investigated including exponential, inverse square and linear. Predictions from each of these were then compared with the earlier experimental measurements.

Using these values for light intensity impacting upon each PMT, the program then transported an appropriately weighted number of photons to each PMT. Finally, an analogue output pulse (including statistical noise) was generated for each event.

An estimate of the location of the event was then determined by intercepting the output pulses of each PMT. After several iterations, an image showing the the results was displayed.

More advanced versions of this program (up to "anger8") increased the capability of the program (as listed in the appendix). Figure 18 shows a flowchart of how the anger program basically works.

The limitations of this program include that it does not

- account for reflections of the edges of the array.
- include the inherit uncertainty due to the electron motion.

Since the data was taken mostly near the centre of the array, and given the exponential drop of photons detected as distance of PMT from beam is increased, the edge effect is small and can be safely ignored. Furthermore, to include motion uncertainties would have caused the program's execution time to become intolerably long.

The Anger programs were used to generate data sets of event mode data which where then analysed by the specific programs, each of which investigated a particular aspect of the detector performance.

CCC was designed to simply calculate the centre of mass of the image, which should be the location of the source.

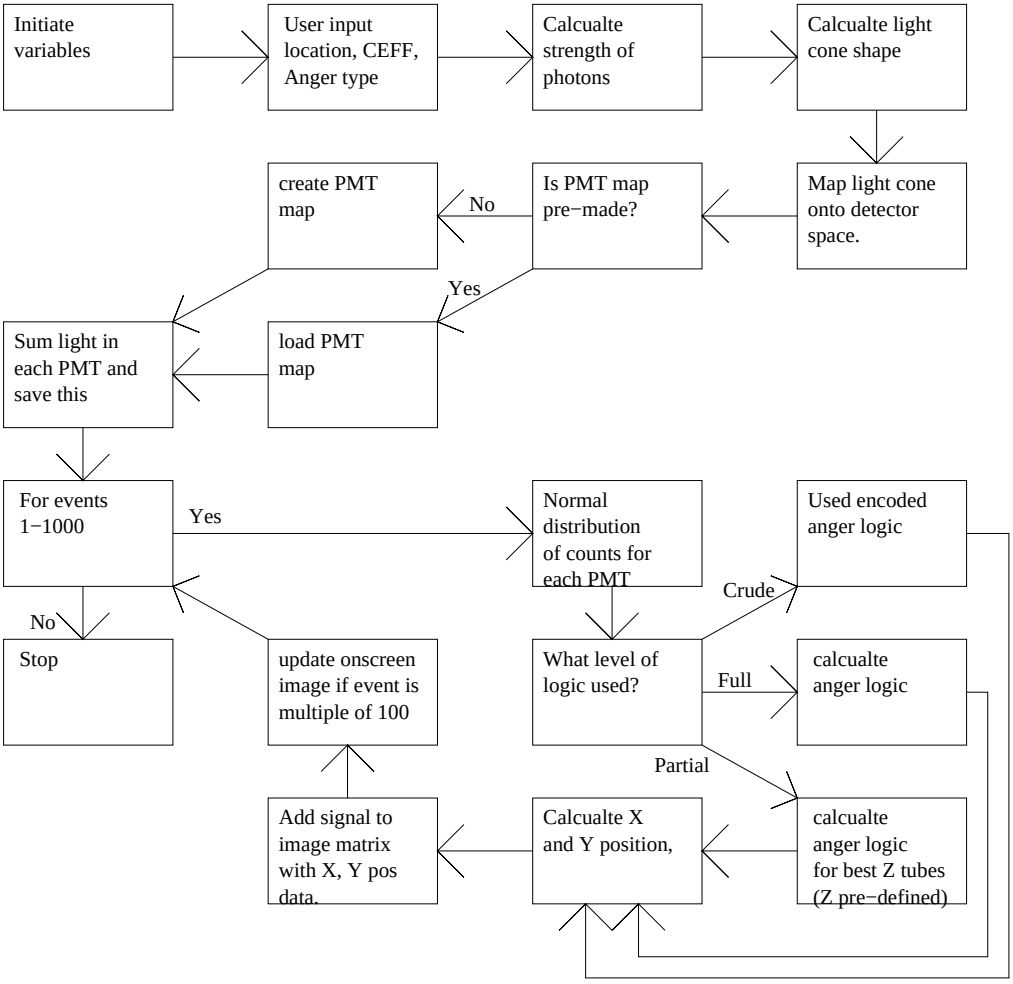

Figure 18: Flowchart of the anger series program.

FWHM calculates the FWHM of an image. It does this by using the image data provided by the anger program and calculating the total light in each pixel of the X and Y directions. If the image data describes the average location as we expect it to, then the FWHM program will obtain an area over which it estimates the location of the source to be and use this as the uncertainty in position.

PileUpChance was designed to calculate the probability of a pile-up event occurring. This program makes the assumption that the length of time that an event is recorded by the PMTs is constant.

4.3 Simulation Work

To match the simulation work with the experimental results as closely as possible, parameters for creating the light cone in simulations was taken directly from the experimental

work. This exponential like decay (figure 16) was used, with some minor changes. As noted, at distances close to the central beam location, the decrease in intensity deviated slightly from a true exponential. This deviation was consider to be marginal and is therefore not included in the simulation.

A series of tests were undertaken to examine the effect of limiting the number of PMTs involved in the position reconstruction algorithm. Figure 19 shows 1000 estimations for a 7 PMT array, at the location of the first measurement. In comparison, figure 20 shows the result obtained when all 49 PMTs in the array are included.

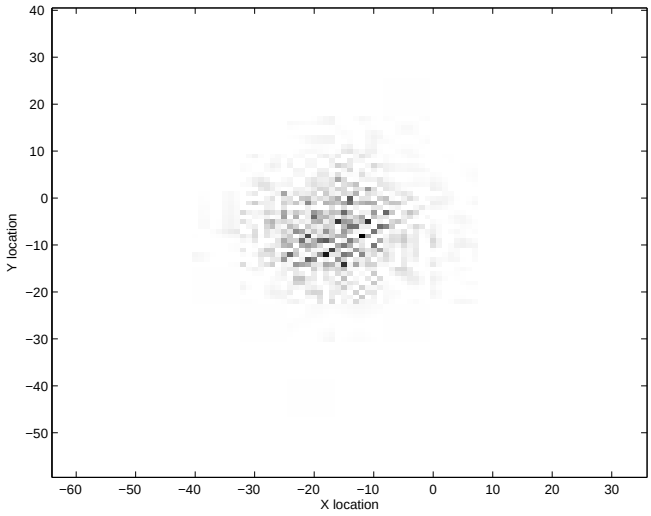

Figure 19: Estimation of location with 7 tube array. Source at (−20 mm, −7 mm).

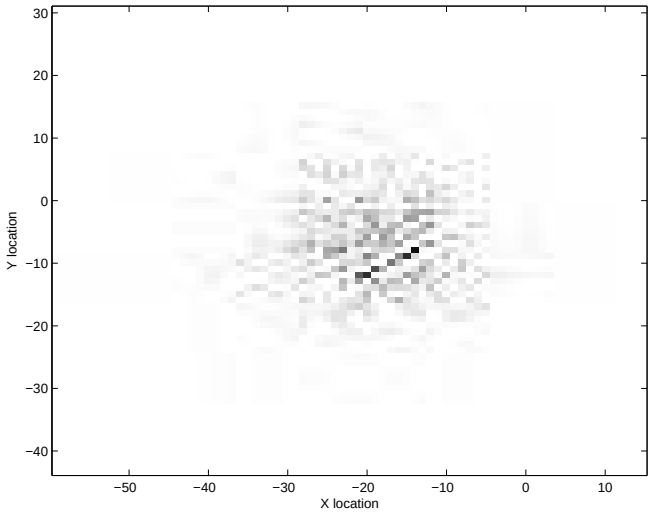

Figure 20: Estimation of location with 49 tube array. Source at (−20 mm, −7 mm).

Estimates of the uncertainties were obtained using the analysis programs described

above and these are shown in the table 4. The data from "ccc" forms the first two entries and "fwhm" gives the second two entries.

	7 tube array	49 tube array
X location estimate (mm)	-16.4	-19.3
Y location estimate (mm)	-5.9	-7.2
X location estimate (mm)	-17.5 ± 7.5	-18.5 ± 8.5
Y location estimate (mm)	-6.0 ± 7	-6.5 ± 6.5

Table 4: X and Y location simulation estimate from a source at (-20 mm, -7 mm)

In both cases, the error in position obtained from the data is large enough to accommodate the experimental observations, but this agreement needs to be carefully considered. For example, the resulting error can quite easily be reduced by increasing the number of photons hitting the detector, or raising the efficiency of the detector.

The simulation was repeated at several locations to test the reliability of the program. At particular locations, some problems were evident as can be seen in 21. At this location, some problems were encountered in attempting to determine the uncertainty in the position reconstruction. Looking at Figures 21 for a 7 tube array and 22 for a 49 tube array, of particular interest is the heavy black line representing a large number of location estimations along it, and the line surrounded by an absence of location estimations (the white in the image) that can been seen in both figures. This is a sign of bias, either in the way that the anger program calculates the location or in the way that it assigns positional randomness. The lines in the image lie along the axis that the PMT's line upon.

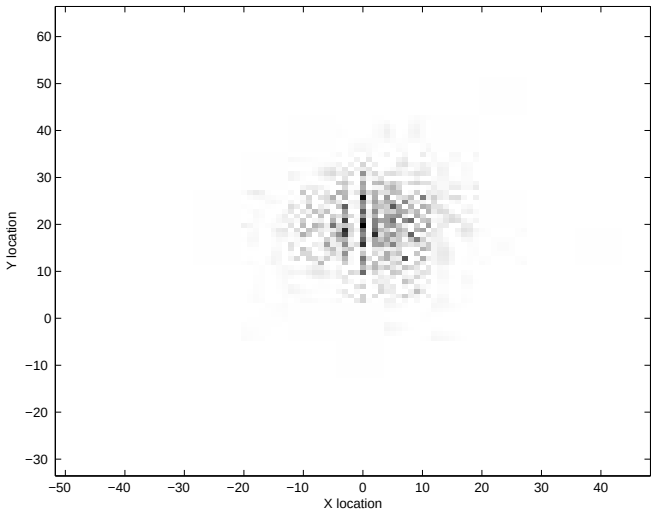

Figure 21: Estimation of location with 7 tube array. Source at (-50 mm, -7 mm), recentred on the PMT with greatest counts.

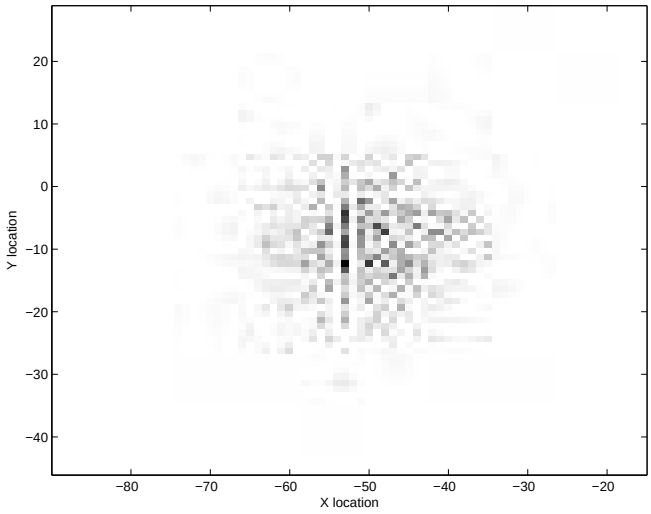

Figure 22: Estimation of location with 49 tube array. Source at (−50 mm, −7 mm).

Looking at Table 5 we see that the bias represented as black lines on the image data show their influence. The first set of data is from the "ccc" calculation and the second set from the "fwhm" calculation. The X location uncertainty is much too small for this case. The reason behind this is how the "fwhm" program calculates the uncertainty from the diagram. This problem can be overcome in several ways. One is to dither the image before estimating the error, but this also increases the uncertainty beyond what it should be, it is hard too calculate how much dithering is needed.

	7 tube array	49 tube array
X location estimate (mm)	-51.8	-50.4
Y location estimate (mm)	-4.2	-8.5
X location estimate (mm)	-53.5 ± 2.5	-52.0 ± 1
Y location estimate (mm)	-4.5 ± 6.5	-6.0 ± 6

Table 5: X and Y location simulation estimate from a source at (−50 mm, −7 mm), with re-centring as needed.

From these tables, we see that the overall effect of increasing the number of PMT analysed is a small decrease in the uncertainity. There is one case (X location estimate at (−20 mm, −7 mm) where the uncertainity actually increased instead. These results show that there are gains, although minimal, that can be made by extension of the Anger logic.

4.4 Pile Up Effects

In a real situation, there is the possibility of two or more photons interacting in the crystal. The final version of the program, "anger8", was developed to investigate this particular

situation. The event generator was modified to accommodate multiple sources (2 at this stage), each with a individual energy and position.

As an example, consider the situation where the previous measurements at (−20 mm, −7 mm) and (−50 mm, −7 mm) are combined. In this case, figure 23 is the result.

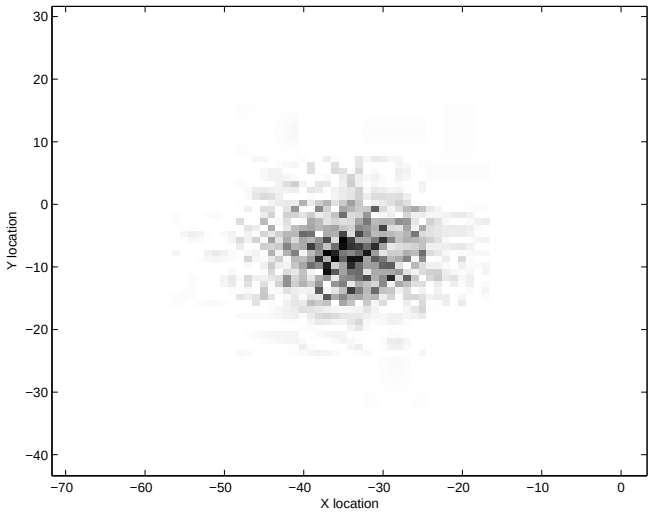

Figure 23: Double source location, sources are at $(-20, -7)$ and $(-50, -7)$.

We can see from this that the location of the two sources gives an estimation of position that is about halfway between the two. From table 6 we see that the suggested location is totally unobservable from this data. This shows the problem that a multiple source situation presents.

	(−20 mm, −7 mm) and (−50 mm, −7 mm)
X location estimate(mm)	-33 ± 6
Y location estimate(mm)	-8 ± 5

Table 6: X and Y location simulation estimate from a source at (−20 mm, −7 mm)

However, provided that the sources are separated sufficiently, it may be possible to resolve the individual events. Once technique would be to examine the data generated by each PMT. As an example, for the case where the two sources are reasonably far apart, a PMT readout like the one shown in figure 24 would be obtained.

In this case we can see that there must be two sources because there is more than 1 local maximum. It needs to be noted that this will not always work, if the two sources are too close together, we will not be able to resolve them. Figure 25 shows this for the first two source case we had. This is the same as in other areas of optical work, such as astronomy, where we might have to objects so close that they are unresolvable. Here, having smaller PMTs would be an advantage that cannot be matched by Anger logic. Another method would be to use pixelated scintillation material, limiting the spread of light cone [Rog99].

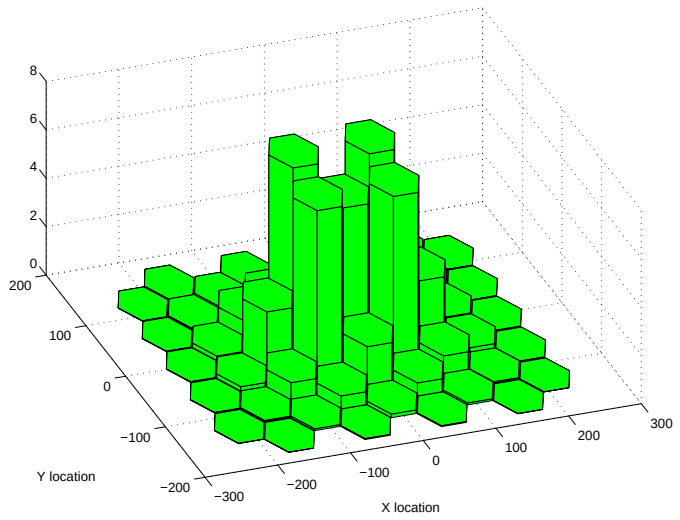

Figure 24: Double source location PMT analysis, sources are at (−50 mm, 0 mm) and (50 mm, 0 mm).

The extent of the adverse effects of pile-up is dependent clearly dependent on count-rates. An attempt was made to test this by generating individual light pulses for each event. Figure 26 shows the flowchart for the pileupchance program. In principle, its operation is straightforward. However, the procedure is computationally intensive and therefore not particularly fast for large numbers of events.

Comparison of the predictions of this model with the experimental measurements is difficult as most of the experimental data was collected at low count rates (≈5 Kps). Under these conditions, and assuming a 230 ns decay constant for NaI together with a 1 μs integration in the electronics results on a moderately low probability of .6262% that a pile-up situation will occur.

4.5 Analysis and Conclusions

The biggest and most important conclusion that we can draw from this is that increasing the number of PMT's analysed in use of Anger Logic provides very little in terms of improved accuracy. Table 4 shows this clearly, where we have a case where increasing the number of tubes and running the simulation again resulted in a larger error than before. Combined with the greatly increased computing power needed and the necessity for it can make calculations quickly when used in the field, this shows that in many cases that it not be useful to increase the range of Anger Logic over the entire array. It should be noted that this is a case of random distributions, but over 1000 iterations, one could reasonably expect the size of uncertainty to be constant.

The "anger" program shows a clear bias when simulating points. It's not known where this bias comes from, but it is easy to see on position estimation graphs that some locations are favoured and others nearby are disfavoured. A result of this is that when the simulated

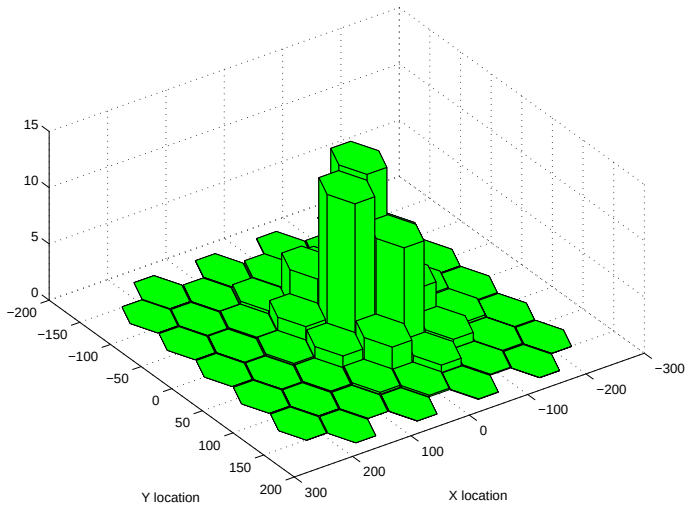

Figure 25: Double source location PMT analysis, sources are at (−20 mm, −7 mm) and(−50 mm, −7 mm).

source is near certain points, the estimate for the uncertainty produced by the "fwhm" is far too low, and certain points are biased against simulating a point.

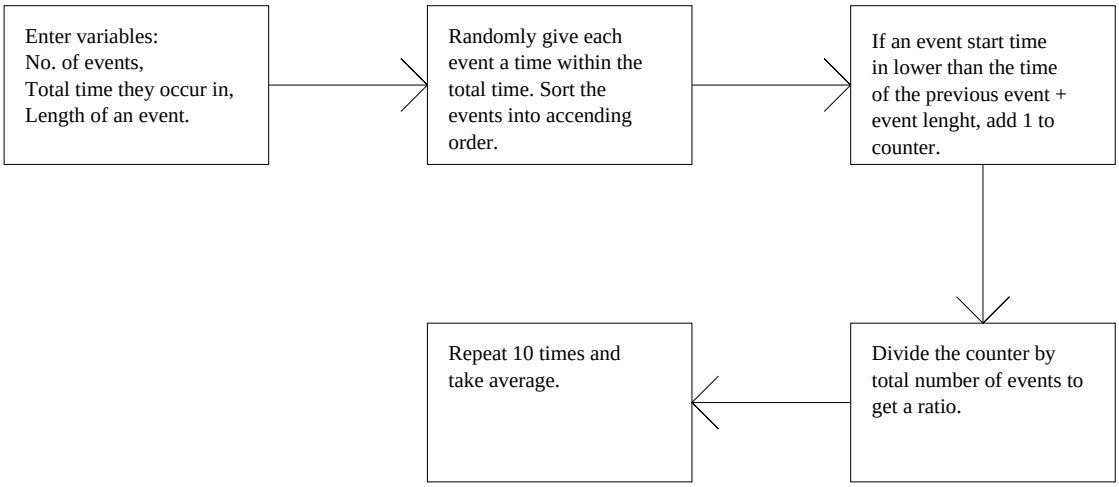

Figure 26: Flowchart of the pileupchance program.

5 Applications

There are several applications for use of gamma cameras. One is the well known, in the area of medical research, with cameras used on patients that have radioactive isotopes injected into their body. With this, structures in their body, like tumours, can be detected. Gamma cameras are not used so much now, falling out of favour to other techniques such as PET (Positron Emission Tomography).

Another, newer, aspect of this work is in the area of explosive detection. The ability to scan areas of ground for land-mines and detect their locations would make clearing areas of mines faster and safer. Figure 27 is what it might look like. Although a slightly different source of radiation would be needed, as well as new problems that arise from it, the principal of detection would be the same. The γ-rays that we would be looking for would be in the range of 10 keV, so the average path length of electrons from this is $\approx 8cm$. With current scintillator thickness, the detector rate would be poor, so it may be necessary to increase the thickness.

Then, using a lead collimator to collect only parallel beams of γ-rays, detection with resolution of order 1 cm should be obtainable. The collimator here would have holes also of 1 cm in diameter in order to be effective at shielding. Since the smallest land-mines tend to be in the order of 5 cm in diameter, this is easily enough to map an area and locate the mines.

Some of the new problems with this are that a neutron source hitting the NaI crystal would also illuminate it, which is what the γ-rays that we are looking for are supposed to do. This has the potential to be a major problem, as the efficiency for such a reaction would be 100% and this background would overwhelm what γ-ray effects we are looking for.

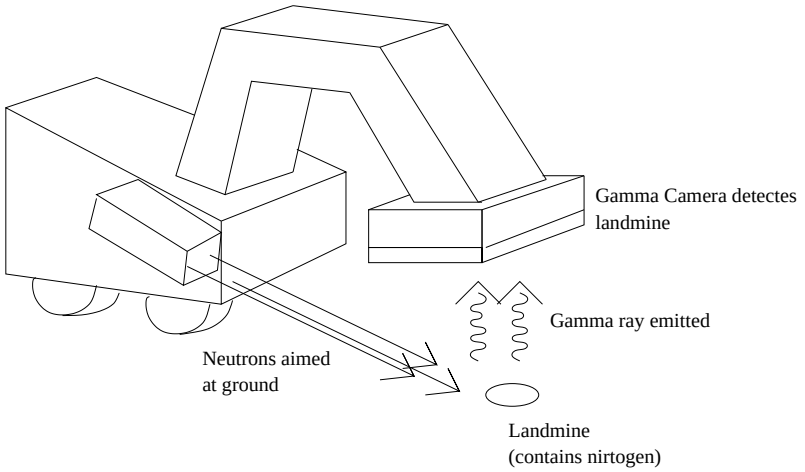

Figure 27: Example of how a gamma camera could be incorporated into a mobile land-mine detector.

6 Summary

This project has carefully measured and modelled the light behaviour of gamma interactions in a large scintillation detector. With this as a basis, possible improvements to position determination have been investigated. Preliminary results suggest that an immediate, although marginal, improvement to position determination can be result from the inclusion of additional PMT events. Although these PMTs, which are a considerable distance from the original point of interaction, carry only a small amount of information, their cumulative behaviour carries valuable information. The inclusion of these additional PMTs will allow the employment of a pulse-pile-up recovery algorithm for high-count-rate applications.

Further refinement to the simulation program will allow direct comparison to be made with experimental measurements. However, the current agreement is sufficient to provide a basis for motivating further work.

A particularly encouraging outcome is that the for the higher energy detection, a resolution of 1 cm is easily achievable without significant hardware modification. This would allow the gamma cameras to be re-deployed as land-mine detectors.

6.1 Further Work

Several areas warrant further investigation. These include:

- Creating a better model of the light distribution to more accurately represent the experimentally measured data. In particular, the observed deviations at distances close to the point of interaction. This could be important to deal will edge effects in the detector.

- A more detailed treatment of the compton events especially for the high-energy application as will be required in the thermal neutron application.

- A thorough investigation of pile-up. As mentioned earlier, under these experimental conditions, it was always extremely small. However, this will not always be the case, so techniques to combat this will be needed. It could become particularly important in the case of land-mine detection as the expected count rate in operation will be close to the detector limit, and consequently the pile-up significant.

A Abbreviations used

FWHM — Full Width at Half Maximum height
MCA — Multichannel Analyser
PMT — Photomultiplier Tube

B Technical Data

B.1 Photomultipler Tubes

Phillips model
Type: XP2422/SL
Date: 17–Aug–92
Batch: 92024

C Properties of Radioactive material

C.1 ^{22}Na

Half-life : $2.602 \pm .002 years$
Radiation : 1274.53 ± 0.02 keV γ-ray, 511 keV γ-ray

C.2 ^{99m}Tc

Half-life : 6.03 hours
Radiation : 123.9 ± 0.7 keV γ-ray

C.3 ^{137}Cs

Half-life : $30.0 \pm 0.2 years$
Radiation : 661.660 ± 0.003 keV γ-ray

D MATLAB Code

The code for these programs is attached to the end of this report.

D.1 anger4 to anger8

Variations of the anger program with improved features in each version.
anger4 - original
anger5 - basic 7 array version
anger6 - basic 49 array version

anger7 - source uncertainty added, but didn't work
anger8 - multi-source

For data in this report, a CEFF of 0.001 was used.

D.2 ccc

Centre of Mass program.

Calculates the Centre of Mass by taking the image data produced from the anger program and weighting it in the normal way. This should give the same results that one would expect if we analyse the image data using Anger logic.

D.3 fwhm

Full With at Half Max height program.

Calculates the Centre of Mass by summing each row and column in the image data and using intensities obtained to plot a graph from which a FWHM can be obtained and the average taken as the middle of this range.

D.4 pileupchance

Calculates pile-up probability by random simulation.

References

[Ang66] H. O. Anger, Sensitivity, resolution, and linearity of the scintillation camera, (IEEE Transactions on Nuclear Science, Vol. 13, 1966)

[Bro86] Edgardo Browne, Richard B.Firestone, Table of Radioactive Isotopes (John Wiley & Sons, Inc 1986)

[NIS] National Institute of Standards and Technology Physics Laboratory (2003) http://www.physics.nist.gov/

[Leo87] W. R. Leo, Techniques for Nuclear and Particle Physics Experiments (Springer-Verlag, Germany, 1987)

[Rog99] Joel G. Rogers and Peter Gumplinger, A Pixelated 3D Anger Camera with Light-Loss Compensation (IEEE Transactions on Nuclear Science, Vol. 46, No. 4, August 1999)

[Sor87] James A. Sorenson, Michael E. Phelps, Physics in Nuclear Medicine Second Edition (W.B. Saunders Company 1987)

[Tho03] M. N. Thompson, R. P. Rassool, Application of Neutron-capture to Elemental Analysis (Physics Review, Vol. 12, Ref. 10, April 2003, University of York)

[Won98] Wai-Hoi Wong, Hongdi Li, Jorge Uribe, A High Count Rate Position Decoding and Energy Measuring Method for Nuclear Cameras Using Anger Logic Detectors. (IEEE Transactions on Nuclear Science, Vol. 45, No. 3, June 1998)